J Mater Sci (2010) 45:3741–3751
DOI 10.1007/s10853-010-4423-6

Evolution of structure and performance of Cu-based layered double hydroxides

L. H. Zhang · F. Li · D. G. Evans · X. Duan

Received: 1 November 2009 / Accepted: 17 March 2010 / Published online: 30 March 2010

Abstract A new series of Cu/Zn/Mn/Fe/Al hydrotalcite-like layered double hydroxides (LDHs) with the Cu/(Zn + Mn)/(Fe + Al) atomic ratios of 1/1/1 in synthesis mixture were synthesized by the coprecipitation method. The chemical composition of multicomponent precursors was identified by chemical analyses. The thermal stability, structure, and texture changes of these as-synthesized LDHs were studied by in situ high-temperature X-ray diffraction (HT-XRD), thermogravimetric-differential thermal analysis combined with mass spectrometry (TG-DTA-MS) in different atmosphere, transmission electron microscopy (TEM), and N_2 adsorption–desorption experiments. The results exhibit that the incorporation of Fe^{3+} and Mn^{2+} into the lattices of Cu-containing LDHs in sequence decreases the crystallinity, water content, and thermal stability of corresponding compounds, and the thermal treatment of LDHs results in the formation of thermodynamically stable composite metal oxide associated with a small amount of simple metal oxide and also changes in texture of calcined solid. Under mild experimental conditions (atmospheric pressure and 25 °C), the catalytic liquid-phase oxidation of aqueous phenol solutions is related to the composition, oxidation states, composite forms and synergy of transition metal cations in calcined LDHs, and calcined LDH with Cu/Zn/Mn/Fe/Al atomic ratio of 1/1/0/0.3/0.7 at 500 °C achieves the highest conversion of phenol mainly owing to the formation of a larger amount of composite metal oxide with some residual carbonate in the solid.

L. H. Zhang (✉)
Department of Catalysis Science and Technology and Tianjin Key Laboratory of Applied Catalysis Science & Technology, School of Chemical Engineering, Tianjin University, Tianjin 300072, People's Republic of China
e-mail: zlh_224@tju.edu.cn

L. H. Zhang · F. Li (✉) · D. G. Evans · X. Duan
State Key Laboratory of Chemical Resource Engineering, Beijing University of Chemical Technology, Beijing 100029, People's Republic of China
e-mail: lifeng@mail.buct.edu.cn

Introduction

Layered double hydroxides (LDHs), $\left[M^{2+}_{1-x}M^{3+}_{x}(OH)_2\right]^{x+}(A^{n-})_{x/n}\cdot mH_2O$, also known as hydrotalcite(HT)-like anionic clay materials, are a family of materials consisting of brucite-like layers [1–3]. As a result of their relative ease of syntheses and flexibility in composition, LDHs have received increased attention in recent years as catalyst supports, catalyst precursors or actual catalysts [3–9].

Thermal decomposition of LDH compounds is a highly significant process for the synthesis of catalysts, and can be characterized by two endothermic transitions [10–12], which depend especially on the chemical composition, crystallinity, and the atmosphere used during decomposition. After dehydroxylation at higher temperatures, the layered crystal structure collapses and predominantly amorphous mixed oxides are obtained, and thus a gradual crystallization of the divalent metal oxides $M^{2+}O$ followed by a $M^{2+}M^{3+}_2O_4$ spinel-like phase can usually be observed in the powder XRD patterns. The ill-organized mixed oxides display generally three broad diffraction maxima corresponding to the future strongest lines of the spinel-like phase, which have large specific surface areas, homogeneous and thermally stable fine dispersion of M^{2+} and M^{3+} (also known as 'non-stoichiometric spinels') on atomic level, and synergetic effects between the elements [10, 13]. The nature/structure of the solids obtained (and

their applications) depends on the starting LDH precursors [14]. In some cases, the transformation of primary oxides and the formation of new oxide phases could be observed at high temperatures [15]. However, the interpretation of the decomposition process is often based merely on the information obtained from ex situ XRD, thermal analysis (TGA combined with DTA or DSC), and gas physisorption experiments [16–18]. Furthermore, most of the studies published on calcined LDHs are carried out at room temperature, where the state of the sample may have changed during cooling, exposure to the atmosphere and handling.

Transition metal oxides, especially those containing copper, have indicated good catalytic properties in catalytic wet oxidation (CWO) of phenol [19–21]. At present, there are many reports on Cu-based and Fe-based oxides as catalysts individually or together employed in oxidation or hydroxylation of aqueous phenol solutions [22–25]. Most notably, more and more attention is being paid to the investigation of Mn-based oxides in the wet oxidation of organic compounds [26]. It is due to their high total organic carbon (TOC) removal [27, 28] and effective suppression of Cu^{2+} ions leaching [29, 30]. The intrinsic properties of the resulting catalysts, like texture, thermal stability, and catalytic properties, might be tuned through controlling the component or composition of precursors [31, 32]. Therefore, it is extremely necessary to study the changes of structure and properties of Cu-containing metal oxides with the incorporation of Fe and Mn element. The preliminary findings about CuZnAl, CuZnFeAl, and CuZnMnFeAl series with different Cu/Zn/Al, Cu/Zn/Fe/Al, and Cu/Zn/Mn/Fe/Al atomic ratio have been reported by us [19, 33–35]. In addition to the atomic ratio, the catalytic performance of Cu-containing mixed oxide catalysts obtained from LDHs also strongly depends on the way of thermal treatment of LDH precursors [3, 36]. In order to investigate in detail the effect of copper, iron, and manganese on the elemental composition, thermal stability, nature of the crystalline phases formed during the thermal decomposition of LDH precursors and texture of the samples calcined at different temperatures, we choose three optimal LDHs with Cu/Zn/Al atomic ratio of 1/1/1, Cu/Zn/Fe/Al atomic ratio of 1/1/0.3/0.7 and Cu/Zn/Mn/Fe/Al atomic ratio of 1/0.7/0.3/0.3/0.7 in synthesis mixture as the object of study of this article. Simultaneously, the catalytic properties of the calcined samples were evaluated by oxidation of aqueous phenol solutions using hydrogen peroxide and were related to the composition and structure of catalysts. To the best of our knowledge, there are no other authors' reports about Cu/Zn/Fe/Al or Cu/Zn/Mn/Fe/Al containing multicomponent mixed metal oxides obtained from LDHs for oxidation of aqueous phenol solutions until recently.

Experimental

Preparation of samples

Cu-LDHs carbonate with the $Cu^{2+}/(Zn^{2+} + Mn^{2+})/(Fe^{3+} + Al^{3+})$ molar ratio of 1/1/1 in the synthesis mixture were prepared by a titration coprecipitation method [19, 33–35]. A mixture inorganic anion solution of NaOH and Na_2CO_3 ($[CO_3^{2-}] = 2[M^{3+}]$, $[OH^-] = 2(2[M^{2+}] + 3[M^{3+}])$) was added dropwise to a metal salts solution of Cu^{2+}, Zn^{2+}, Mn^{2+}, Fe^{3+}, and Al^{3+} (total cation concentration of 1.2 mol/L) depending upon the Cu/Zn/Mn/Fe/Al atomic ratio with vigorous stirring until the solution pH value up to 10.0. The slurry thus obtained was aged at 60 °C for 10 h under stirring, then filtered and washed with deionized water until the pH of the filtrate was around 7 (aim at eliminate the alkali metal and the nitrate ions). For the Mn-containing sample, these processes were manipulated under nitrogen atmosphere, even the deionized water was also treated by nitrogen. The filter cake was dried at 60 °C in an air oven overnight. The corresponding samples were calcined at 300, 400, 440, 500, 600, and 700 °C for 3 h. For the purpose of convenience, the LDH precursors with Cu/Zn/Mn/Fe/Al atomic ratios of 1/1/0/0/1, 1/1/0/0.3/0.7, and 1/0.7/0.3/0.3/0.7 in the synthesis mixture were denoted as Cu-LDH1, Cu-LDH2, and Cu-LDH3, respectively.

Characterization

X-ray power diffraction (XRD) patterns were obtained with a Shimadzu XRD-6000 X-ray diffractometer by 40 kV, 30 mA, Ni-filtered Cu Kα radiation ($\lambda = 1.5406$ Å) with a scan speed of $2\theta = 5^\circ$/min. Structural evolutions during thermal treatment under air were carried out by in situ high temperature powder X-ray diffraction (HT-XRD) attachment in the temperature range 30–800 °C.

Elemental analysis was performed by an inductively coupled plasma emission spectrometer (ICP-ES) of Shimadzu ICPS-7500 model. Samples were dried at 100 °C for 24 h prior to analysis, and solutions were prepared by dissolving the samples in dilute hydrochloric acid (1:1). C, H, and N microanalysis was obtained on an elemental analyzer (EA) of Elementar Analysensysteme GmbH Vario El model.

Thermogravimetric and differential thermal analysis (TG-DTA) were carried out using a Seiko 6300 TG/DTA/DSC synchronization thermal analyses apparatus at a heating rate of 10 °C/min in both a synthetic dry air stream (78% N_2, 22% O_2-flux of 180 mL/min) and nitrogen (200 mL/min). Simultaneous analysis of the evolved gases was continuously monitored with a quadrupole mass spectrometer ThermoStar^{TM} QMS 200 connected on-line to the microbalance by a quartz capillary transfer line at 190 °C to prevent the condensation of evolved gases.

The specific surface area determination and pore volume analysis were performed by BET and BJH methods using a Quantachrome Autosorb-1C-VP Analyzer. Prior to the measurements, samples were degassed at 200 °C for 2 h.

Transmission Electron Microscopy (TEM) studies were performed using a Hitachi H-800 model machine for high-resolution observation. The accelerating voltage applied was 100 kV. Specimens for TEM were prepared by standard techniques.

Catalytic reactions

The catalytic oxidation process was carried out in a 250 mL three-neck glass flask. Hydrogen peroxide solution (30% w/v, 1 mL) was added to an aqueous phenol solution (100 mg/L, 100 mL) containing 0.2 g of catalyst. The mixture was kept at room temperature for 60 min. The phenol conversion and product distribution were determined by HPLC. Aliquots of 5 μL were injected into a reverse-phase C-18 column, with a mixture of 30% methanol and 70% of redistilled water as a mobile phase at a total flow rate of 0.8 mL/min. The absorbance at 280 nm was used to measure the concentration of phenol.

Results and discussion

In situ HT-XRD study

The determination of crystalline phases formed during calcination at various temperatures is useful to understand the thermal stability of the compounds. In situ HT-XRD patterns of Cu-LDHs in the temperature range 30–800 °C are shown in Fig. 1. Obtained results at room temperature reveal that as-prepared samples have a hexagonal structure with peaks characteristic of hydrotalcite(HT)-like materials [3], exhibiting sharp and symmetric Bragg reflections of the basal (003), (006), and (009) planes, and broad and asymmetric reflections for the non-basal (012), (015), and (018) planes. The (009) and (012) reflections overlap results in the broad signal between 32° and 38° at 2θ angles. Furthermore, the two reflections of (110) and (113) can be clearly distinguished around 60° at 2θ angles. The comparison of XRD peak's intensities of three LDHs samples shows that the crystallinity decreases in these LDH precursors from samples Cu-LDH1 to Cu-LDH2 and to Cu-LDH3. It is likely because of the decreasing stacking of the layers with the incorporation of more and more metal ions. It should be emphasized that the colors, influenced by structure characteristics and transition metal ions, for Cu-LDH1, Cu-LDH2, and Cu-LDH3 are light blue, brown beige, and sepia brown, respectively.

Table 1 summarizes the analytical and structural data of three precursors. For every sample, LDH phase is the single crystalline phase detected by XRD. The theoretical formulas of all the samples are also given in Table 1 on the basis of the results of chemical analyses, water content estimated from the mass losses in the first step of TG curves recorded in nitrogen (see below) and the rule of charge balance. The final M^{2+}/M^{3+} ratios in the synthesis LDHs are significantly higher than those (=2) in the initial synthesis mixtures. The result should be mainly attributed to the depletion of amphoteric aluminum hydroxide precipitate by re-dissolving at the high pH (=10.0) of the medium. The decrease of the final M^{2+}/M^{3+} ratios with the increase of metal species in samples declares that the increase of positive charge density in the layers. It is just this reason makes the M^{2+}–M^{3+}–O octahedron shrunken and results in the reduction of lattice parameter a [1–3]. It is clear that the results of EA as well as the values of basal spacing (d_{003}) together prove that the planar CO_3^{2-} is the only guest anion in the interlayer. Under the same arrangement of CO_3^{2-} in the interlayer galleries and minimum molecular formulas, the decrease of interlayer water content with the increase of metal species in samples can be predicated from the increasing interlayer CO_3^{2-} with the decrease of lattice parameter c.

Thermal treatment of the samples has resulted in the changes of their chemical composition, phase content, and color. It should be noted that in the patterns at 100 °C, the intensity of the (003) and (006) peaks becomes weak. The resolution of the doublet close to 60° at 2θ angles is also worse, and the (113) reflection vanishes at 120 °C, while the intensity of the (110) reflection diminishes significantly, becoming broader. In the pattern at 180 °C for Cu-LDH1, 160 °C for Cu-LDH2, and 140 °C for Cu-LDH3, only the (003) reflection of the LDH phase is visible with reduced intensity. This suggests the formation and growth of some amorphous phases in the process of the decomposition of layered structure. Meanwhile, the (003) diffraction peak of the samples moves to higher 2θ angle with increasing temperature and the value of d_{003} decreases in one step as shown in Fig. 2. According to the literature [37] and the TG-DTG-MS results discussed below, the phenomenon can be attributed to the gradual removal of physically adsorbed water and interlayer water from the LDH materials, which causes a slight decrease in the interlayer spacing. Anyway, it can be concluded that the samples partially retain a layered structure at these temperatures, with similar metal–metal distances in the layers as in the precursors [38]. However, the disappearance of (006) and (009) planes indicates that some stacking disorder is involved in the stacking sequence, as previously stated by other authors [39, 40]. The loss of the interlayer water destabilizes the structure of LDHs. And the layered structure completely

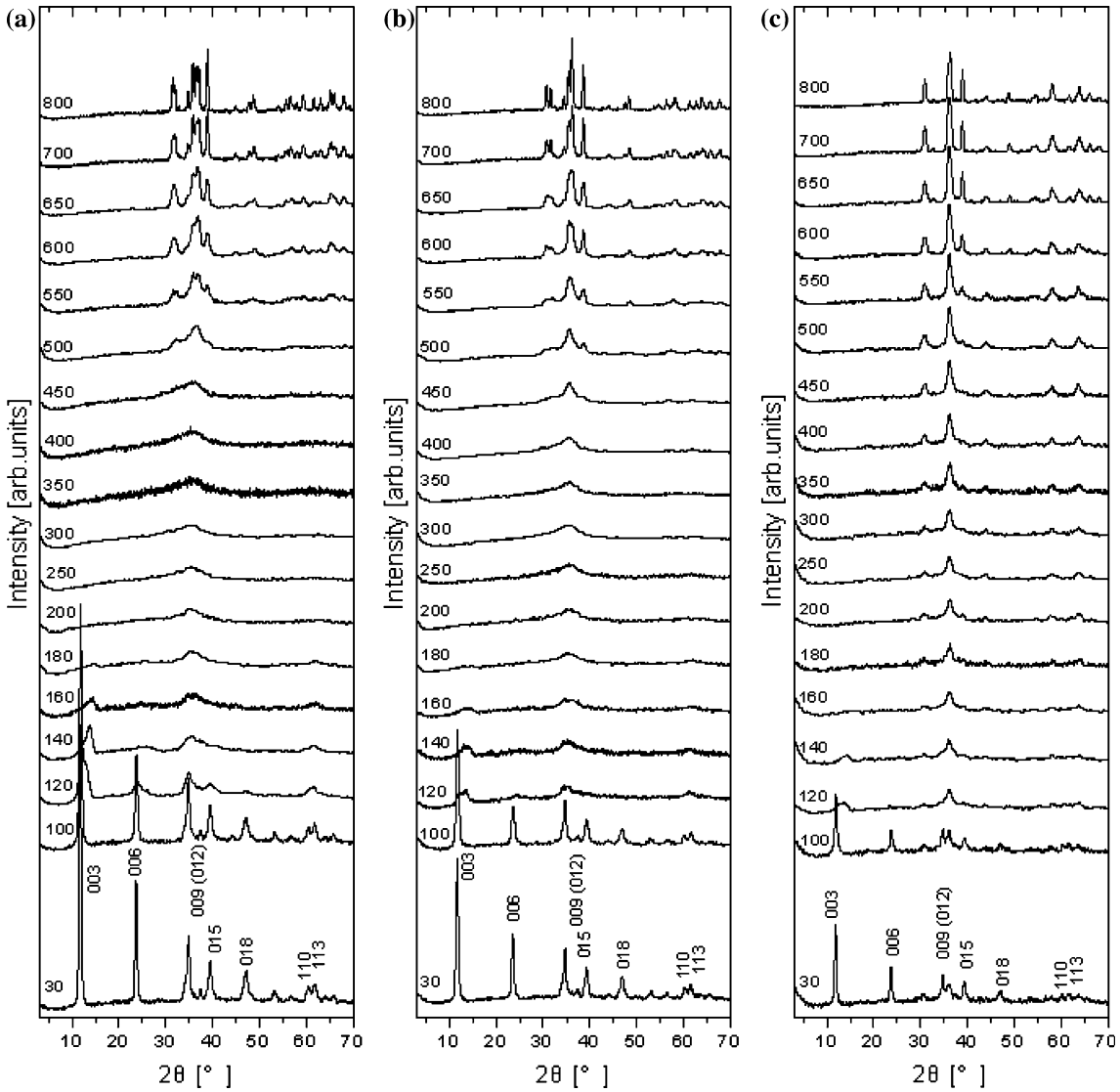

Fig. 1 The HT-XRD patterns for the thermal decomposition of **a** Cu-LDH1, **b** Cu-LDH2, and **c** Cu-LDH3

Table 1 Analytical and structural data for as-synthesized samples

Sample	Theoretical formula for LDH[a]	M^{2+}/M^{3+} ratio[a]	XRD phase[b]	d_{003} (Å)	a^c (Å)	c^d (Å)
Cu-LDH1	$Cu_{0.357}Zn_{0.357}Al_{0.286}(OH)_2(CO_3)_{0.143}\cdot 1.10H_2O$	2.50	LDH	7.58	3.07	22.75
Cu-LDH2	$Cu_{0.351}Zn_{0.361}\ Fe_{0.095}Al_{0.193}(OH)_2(CO_3)_{0.144}\cdot 0.97H_2O$	2.48	LDH	7.50	3.07	22.49
Cu-LDH3	$Cu_{0.350}Zn_{0.252}Mn_{0.101}Fe_{0.094}Al_{0.203}(OH)_2(CO_3)_{0.149}\cdot 0.89H_2O$	2.36	LDH	7.46	3.06	22.40

[a] Chemical analyses results obtained from ICP-ES and EA

[b] LDH = layered double hydroxide

[c] Lattice parameter a (= $2d_{110}$)

[d] Lattice parameter c (= $d_{003} + 2d_{006} + 3d_{009}$)

collapses at a temperature of 200 °C for sample Cu-LDH1, 180 °C for Cu-LDH2, and 160 °C for Cu-LDH3, due to the release of structural water and CO_2 from the interlayer. The process of thermal treatment is useful for inducing crystal growth in amorphous phases and formation of composite metal oxides (poorly crystallized spinel-like mixed oxide) containing corresponding transition metal ions, as indicated by sharpening of the XRD lines. Obviously, the phase

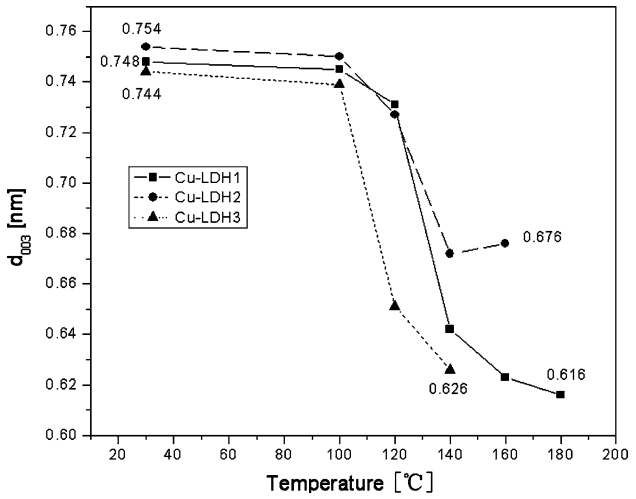

Fig. 2 Variation of the d_{003} basal spacing of the samples as a function of calcinations temperature

transition temperature from LDHs to oxide-type and/or spinel-type containing the different transition metal ions always decreases in the order Cu-LDH1, Cu-LDH2, and Cu-LDH3. The introduction of transition metal in the LDHs influenced strongly the phase composition of the calcined samples and the thermal stability of LDHs precursors. With further increase in the calcination temperature from 650 to 800 °C, the spinel-like phase is still the only detectable phase in the Mn-doped sample. However, some simple oxide phases, such as CuO and ZnO, can be identified together with the composite metal oxide phase in calcined Cu-LDH1 and calcined Cu-LDH2. All these results arise from the increasing metal–oxygen bond (M–O) strength from Cu–O to Fe–O and to Mn–O (Cu–O approximately 255 kJ/mol, Fe–O approximately 398 kJ/mol, and Mn–O approximately 402 kJ/mol [41]). On the other hand, the heats of formation of a mole of the composite metal oxide $MnO{\cdot}Al_2O_3$, $MnO{\cdot}Mn_2O_3$, $MnO{\cdot}Fe_2O_3$, $ZnO{\cdot}Fe_2O_3$, $CuO{\cdot}Fe_2O_3$, and the simple metal oxide Mn_2O_3, Fe_2O_3, MnO_2, ZnO_2, CuO are −2104.55, −1386.58, −1226.33, −1178.63, −967.97, −956.88, −825.50, −520.07, −348.11, and −155.85 kJ/mol, respectively [42, 43]. The decreased tendency implies that the formation of the stable composite metal oxides is preferred compared with the simple metal oxides in the calcined solids and the Mn is the first element that can be transformed into oxides, after that, Fe and Zn are utilized. The above analysis also explains why the thermal stability of precursors decreases in accordance with the order of Cu-LDH1, Cu-LDH2, and Cu-LDH3. Certainly, the composition of the composite metal oxide is not only binary. Cu and residual Zn and Al elements also can be incorporated into the composite metal oxides with indefinite composition and atomic ratio. In any case, the CuO and ZnO are the possible simple metal oxide phases due to the low heat of formation and high atomic ratio in precursors (see Table 1). Combined with TEM images in the temperature range 400–500 °C, we find that there exist the simple metal oxides in solids. These simple metal oxide phases are highly dispersed on the surface of the composite metal oxides so they cannot be detected by XRD. In general, it is beneficial to the growth of oxide crystal by enhancing the calcination temperature. Indeed, a visible growth tendency of the composite metal oxide crystals can be deduced from the decreased peak half-width for every sample calcined from ca. 500 to 800 °C (see in Fig. 1). The same tendency can be found for the simple metal oxides in calcined Cu-LDH1 and Cu-LDH2. While, it is difficult to distinguish between the simple metal oxides and spinel phases in calcined Cu-LDH3 from XRD pattern at high temperature. This presumably due to the formation of a solid-solution contained with ZnO and CuO in calcined Cu-LDH3. Just as Predicted, the colors of all samples become more and more dark with rising temperature, and almost black after calcination above 600 °C. The color change also demonstrates that the structural transformations occur on heating.

TG/DTA-MS study

Decomposition of Cu/Zn/Mn/Fe/Al-LDH samples under a synthetic dry air atmosphere is followed by thermogravimetry from 30 to 800 °C. The nature of the gases released during the thermal treatment was monitored by mass spectrometry (MS). Plots of the mass loss and differential mass loss as a function of temperature are given in Fig. 3, as well as the MS data.

According to the results of TG-DTG-MS and the reports about the thermal decomposition of LDHs [1, 44–46], the mass losses can be divided into three stages for every sample, commonly involving the rapid removal of the interlayer and weakly adsorbed water in the low-temperature range (ca. 30–200 °C) followed by the slow dehydroxylation of the brucite-like layers and the partial decarbonation up to 500 °C. While the release of residual large amount of anions (CO_3^{2-}) and small amount of hydroxyl groups is mainly in the range of 500–780 °C. It is necessary to emphasize that NO_2 and CO_2 are released at the same temperature, but the signal intensity of CO_2 is very stronger than that of NO_2 irrespective of the incorporation of Fe^{3+} and even Mn^{2+} ion. Taking into account of the results of XRD and EA, the appearance of nitrogen oxides in the evolved gases during thermal decomposition should be attributed to the oxidation of nitrogen from air.

It can be seen that the DTG peaks center are all shifted to lower temperature from sample Cu-LDH1 to Cu-LDH2 and to Cu-LDH3 in Fig. 3 which indicating the thermal stability of their layer structure is decreased with Al^{3+} and Zn^{2+} ion being partially substituted by Fe^{3+} and Mn^{2+} ion,

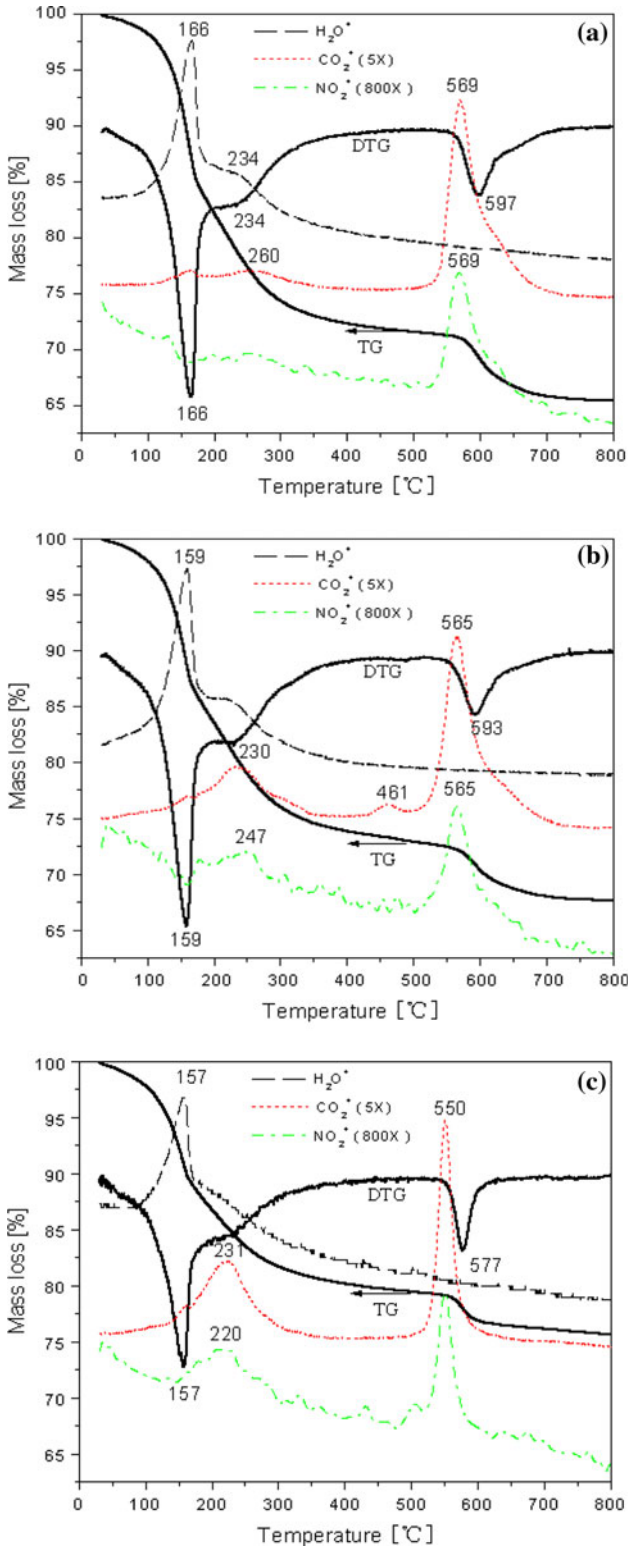

Fig. 3 The TG-DTG-MS for **a** Cu-LDH1; **b** Cu-LDH2; and **c** Cu-LDH3 recorded in synthetic air

respectively. As a result, the removal of interlayer water, dehydroxylation of the lattice, and decomposition of the interlayer CO_3^{2-} anions are apparently more facile for sample Cu-LDH3, as these events occur at lower temperatures than those observed for other two samples. This is also indicative of a decrease in the strength of hydrogen bonds between water molecules and interlayer anions, and thus a reduced electrostatic interaction between the layers and the anions, which facilitates the process for mass loss, thus the structural transformation [47]. It also can be explained by the differences in bond energy for Cu–O, Fe–O, and Mn–O. The metal ion with high M–O bond energy and lying in octahedral center can greatly strengthen polarity of intralayer OH^- linked to it and reduce H-bond attractive force between the layers and the interlayer anions and water molecules, and even weaken the thermal stability of intralayer OH^-, thus resulting in the decreasing thermal stability of layer structure going from sample Cu-LDH1 to Cu-LDH2 and to Cu-LDH3. Besides, the octahedral crystal field stabilization energy (CFSE) of metal ions also affects the thermal decomposition of LDHs [48, 49]. It is well known that the octahedral CFSE of high spin d^5 configuration of Fe^{3+} and Mn^{2+} ion is equal to zero. Compared to the Jahn–Teller Cu^{2+} ion (CFSE $\neq$ 0), the incorporation of these ions into the layer will facilitate the deformations of the O–M–O bond angles and lead to the facile thermal decomposition of the LDHs. Further, as discussed in HT-XRD section, the heat of formation of a mole of Mn-containing metal oxide is the highest followed by Fe-, Zn-, and Cu-containing metal oxide. The higher the heat of formation of a mole of metal oxide, the more stable the formed metal oxide. It also predicts that the thermal stability of precursors decreases following the order: Cu-LDH1 > Fe-containing Cu-LDH2 > Fe- and Mn-containing Cu-LDH3. The thermal decomposition behaviors of these samples in nitrogen shown in Fig. 4 are similar to those in synthetic air.

The in situ HT-XRD experiments provide information about the structural changes during thermal treatment under a synthetic dry airflow. Taking example for the structural evolution of sample Cu-LDH1 calcined at 160 °C reported in Fig. 1a, the results from the in situ XRD experiments are in agreement with the TG/DTG-MS profiles of the samples calcined at 160 °C, showing a maximum in the mass loss rate between 30 and 200 °C, which appears well correlated with the progressive decomposition of samples.

Figure 5 shows the DTA patterns for the Cu/Zn/Mn/Fe/Al-LDHs recorded in synthetic air and in nitrogen. The peak positions and shapes of the DTA curves are almost identical to those of the DTG curves up to ca. 300 °C. It implies that the mass loss processes reflected in TG (DTG) are associated with endothermic transformations observed in DTA. It is important to find out some minor differences in these profiles. The first DTA peak, due to dehydration, is nearly similar in all cases, while the second effect is much weaker when the analysis is performed in synthetic air and

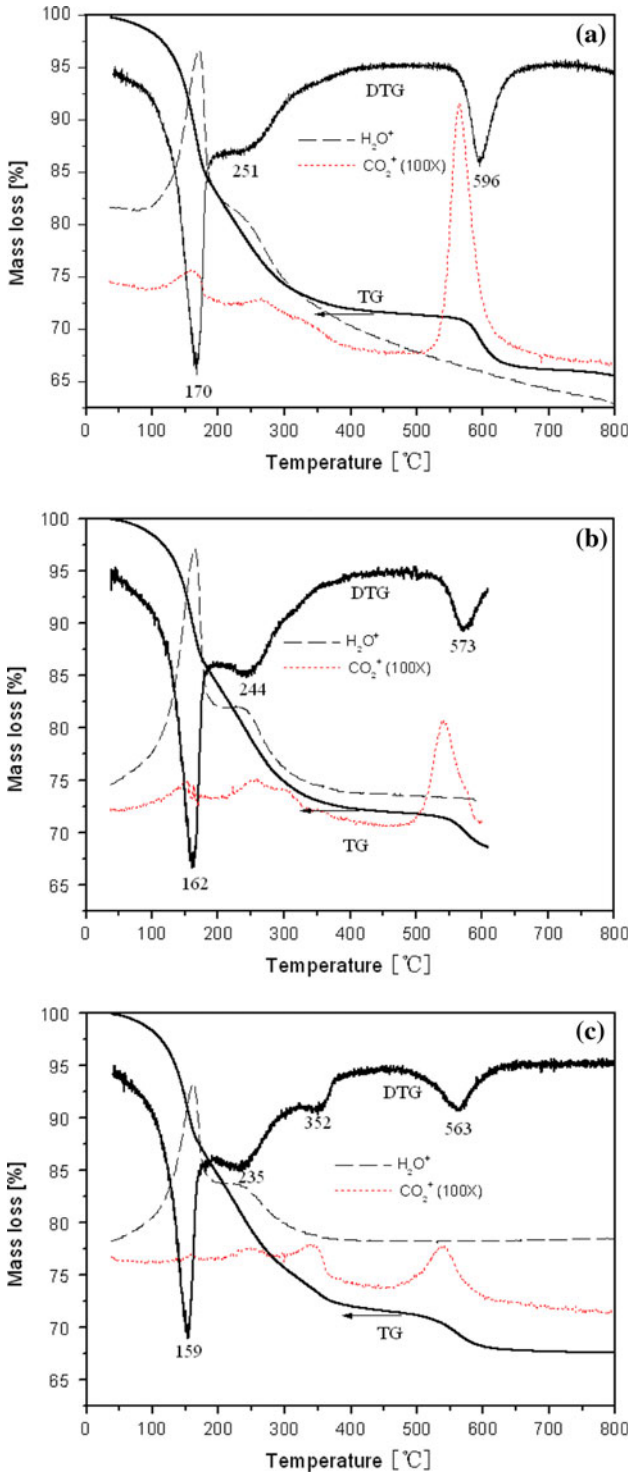

Fig. 4 The TG-DTG-MS for **a** Cu-LDH1; **b** Cu-LDH2; and **c** Cu-LDH3 recorded in nitrogen

shows a rather expected intensity when recorded in nitrogen. This behavior is undoubtedly related to the presence of transition metal ions with various oxidation states and composite forms [19, 33, 50–53]. During calcinations in air, the transition metal ions in precursors are more easily

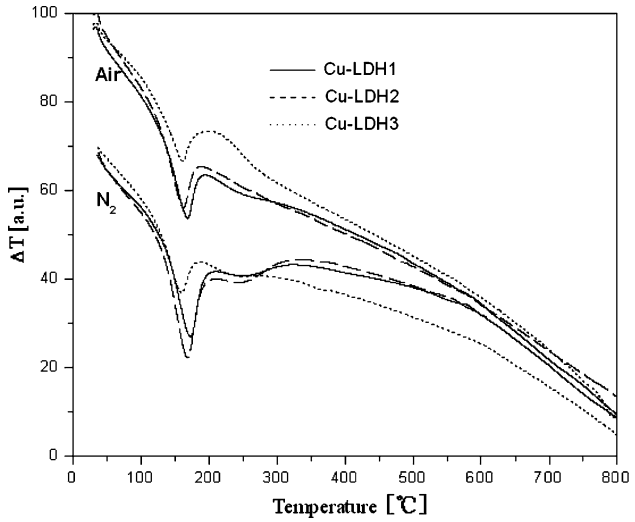

Fig. 5 The DTA curves for the Cu/Zn/Mn/Fe/Al-LDHs samples recorded in nitrogen and synthetic air

transformed into high valence and thermodynamically stable oxides which accompanying heat release. It means the heat of reaction in air is higher than that in nitrogen. The exothermic process presumably takes place in the same temperature range as the endothermic removal of hydroxide and carbonate and the endothermic effect in air can obtain more thermal compensation from the exothermic effect than that in nitrogen [54]. Note that there is no any thermal effect signal for DTA curves above ca. 300 °C coupled with mass losses recorded above this temperature. It suggests that the endothermic effect of decarbonation is completely offset by the exothermic effect of structural rearrangement due to their opposite signs in the high temperature [44, 55]. Moreover, the temperature recorded in the DTA analysis is lower when the analysis is performed in synthetic air than that in nitrogen. It is just due to the calcinations of the Cu-LDHs in air more easily lead to the formation of metal oxides than that in nitrogen, which result in the low stability of sample in air.

The mass losses for samples are included in Table 2. In all cases, every stage mass losses are calculated, the inflexion points of which coincide with the DTG curve and the line of ion current for H_2O^+. As the first mass loss is attributed to the removal of the interlayer and weakly adsorbed water [56], their determination can be straightforwardly carried out and the values are listed in the first column of Table 2. The water content decreases from Cu-LDH1 to Cu-LDH2 and to Cu-LDH2 irrespective of atmosphere. The change confirms the prediction from lattice parameter *c*. It is more likely ascribed to the increasing binding energy of hydrated cation in accordance with the order of 326.74 kcal/mol for Mn^{2+} ion, 352.74 kcal/mol for Zn^{2+} ion, 697.09 kcal/mol for Fe^{3+} ion, and 730.47 kcal/mol for Al^{3+} ion [57]. The higher binding energy of hydrated cation, the more easily to

Table 2 Data of the thermo-gravimetric analysis of the samples in synthetic air and in N_2

Sample	Weight loss stage (wt%)							
	I		II		III		Total loss	
	Air	N_2	Air	N_2	Air	N_2	Air	N_2
Cu-LDH1	18	17	11	12	6	6	35	35
Cu-LDH2	16	15	11	13	5	–	32	–
Cu-LDH3	12	14	9	15	4	3	25	32

combine the water molecule with metal cation. The mass loss difference for Cu-LDH3 in air and nitrogen may be arising from the facile oxidation of Mn^{2+} ion in air. In the middle stage, the mass losses of Cu-LDH1 are still nearly identical in the different atmosphere. However, the mass losses of Cu-LDH2 and Cu-LDH3 in air are lower than that in nitrogen and the difference is enlarged for Cu-LDH3. The reason is that the increasing mass due to the facile oxidation of Fe^{3+} and Mn^{2+} ions in air can partially offset the mass loss in the thermal treatment process of Cu-LDH2 and Cu-LDH3. In nitrogen, an increase mass loss in the second stage and a decrease mass loss in the third stage can be observed in accordance with the order of Cu-LDH1, Cu-LDH2, and Cu-LDH3. At the same time, the MS peak area ratio for CO_2^+ in the second stage to that in the third stage for Cu-LDH3 is the highest followed by Cu-LDH2 and Cu-LDH1 (see Figs. 3, 4). These results further imply that the introduction of Fe^{3+} and Mn^{2+} ion makes the elimination of the interlayer CO_3^{2-} easier and the thermal stability of the LDHs structure weaker. It is just the slight decrease of water content and increase of oxidation states of Fe and Mn element [19, 42–46] taking place in air, lead to the decrease of the total mass loss in air with the introduction of Fe^{3+} and Mn^{2+} ion. The above results coincide with the DTG and DTA results. In order to trace changes taking place during calcination in air, we have recorded TEM, BET, and catalytic activity tests at selected temperatures corresponding to points at in situ HT-XRD and TG-DTG-MS profiles above 300 °C in air and corresponding results and discussion are reported in what follows.

TEM imaging analysis

The changes of the samples texture depending on the calcination temperature also can be seen in the TEM images in Fig. 6. Except that the in situ XRD pattern of the dried Cu/Zn/Mn/Fe/Al-LDHs samples exhibited HT-like type diffraction lines, the thin platy crystals characteristic for LDHs compounds also can be distinguished in the TEM images. These crystals were destroyed during thermal treatment at high temperature. Judging from the morphology in TEM and structure analysis in XRD, the composite

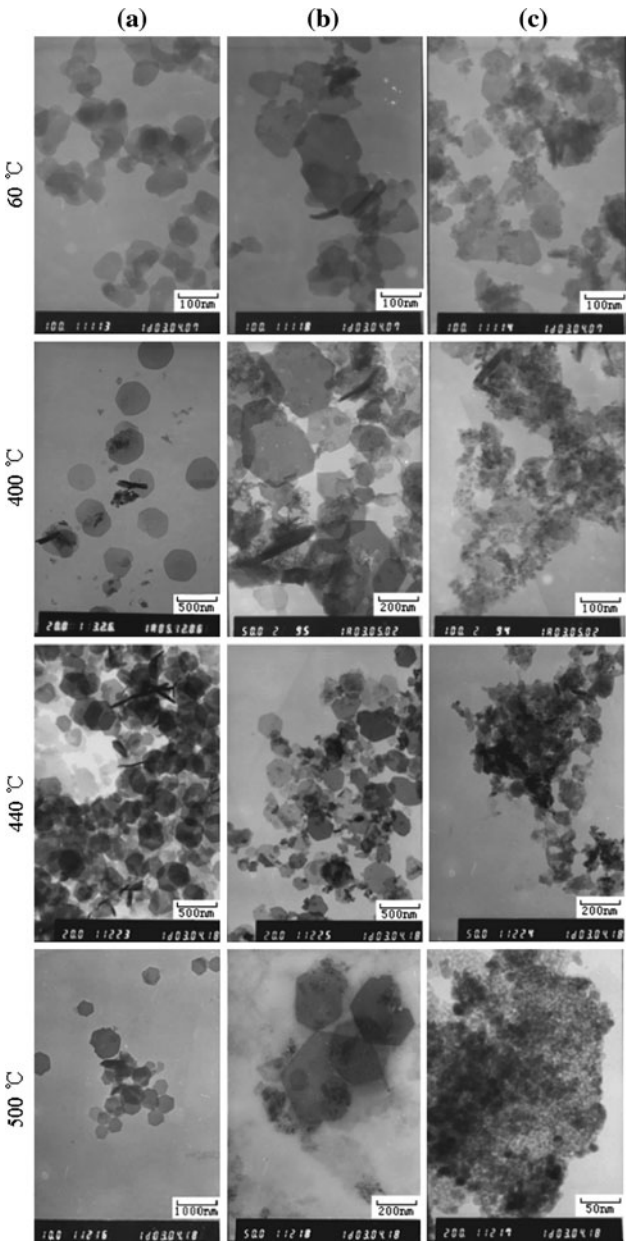

Fig. 6 TEM images of **a** Cu-LDH1; **b** Cu-LDH2; and **c** Cu-LDH3 calcined at different temperature

metal oxide phase coexists with the simple metal oxide phase in calcined solids and the more part is the composite metal oxide phase. Obviously, the morphology of the composite metal oxide in calcined Cu-LDH3 is significantly different from the hexagonal platelet nature of the composite metal oxide in calcined Cu-LDH1 and Cu-LDH2 in the TEM micrographs [19]. The difference is related to the partial substitution of Zn^{2+} ion by Mn^{2+} ion in precursor which leads to the different structure characteristics of composite metal oxide phase. The sizes of Cu-LDH1 and Cu-LDH2 calcined at 400, 440, and 500 °C are nearly similar and larger than that of the corresponding

samples dried at 60 °C. However, the average grain size of calcined Cu-LDH3 is obvious smaller than that of its precursor and other samples at the same temperature, which is responsible for its high specific surface area compared with calcined Cu-LDH1 and Cu-LDH2.

Textural properties

The specific surface areas (SSAs) of the samples calcined at different temperatures (400–700°C) in air, as well as their pore volumes, have been measured from the corresponding nitrogen adsorption–desorption isotherms at −196 °C. The changes in these variables with the calcinations temperature have been listed in Table 3. It can be seen that there is no obvious variation for the SSAs of calcined sample Cu-LDH1 in the region 400–700 °C. Among them, the maximum change range is 7 m^2/g. Below 500 °C, the SSAs for calcined sample Cu-LDH2 are higher than that of the sample Cu-LDH1 and the change range is less than 4 m^2/g. After calcination at 600 °C, the SSA for calcined sample Cu-LDH2 is reduced nearly one half and even the value is reduced to 23 m^2/g at 700 °C. Similarly, the high SSAs of 107, 90, and 245 m^2/g for sample Cu-LDH3 calcined at 400, 440, and 500 °C, respectively, can be suddenly dropped to 57 m^2/g at 600 °C and even 33 m^2/g at 700 °C. Another significant difference from other two samples is the obvious fluctuation of the SSA below 500 °C. In any cases, the variation in total pore volume is nearly parallel to that in SSA. Usually, the removal of H_2O and CO_2 from the interlayer can form craters on the surface [58, 59] and improve the pore volume and surface area. Below 500 °C, the fluctuation of the SSA and total pore volume implies that the structural transformation also can influence the textural properties. Above 600 °C, the sharp decrease of the SSA and the total pore volume for calcined Cu-LDH2 and Cu-LDH3 is related to the sintering and the formation of spinel-like phases. The estimation is on the basis of previous results, especially in situ HT-XRD patterns. As shown in Fig. 1, the diffraction peaks for Cu-LDH2 and Cu-LDH3 calcined at 600 and 700 °C become narrow which suggestive of increased crystallinity and crystallite size. For Cu-LDH1 calcined at 600 and 700 °C, it is just the small simple metal oxides coupled with spinel-like phases keep the nearly invariable SSAs. Compared with each other, we can find that the introduction of Fe^{3+} and Mn^{2+} ions into brucite-like sheets of samples Cu-LDH1 results in a sharp increase of its surface area observed after calcinations at 500 °C from 44 to 76 and to 245 m^2/g, depending on the different structure nature resulting from the cooperative effect between the different metallic elements.

Catalytic activity

Oxidation of phenol was carried out on these Cu/Zn/Mn/Fe/Al-LDHs samples calcined at different temperatures for 3 h, and the results are summarized in the last column of Table 3. It can be seen that there is a maximal value for the observed activity exhibited by each sample calcined at intermediate temperature, such as 500 °C for Cu-LDH1 and Cu-LDH2 or 440 °C for Cu-LDH3. According to our previous studies [19, 34, 35], the high conversion is correlated to the formation of a great amount of composite metal oxide with indefinite composition in the solid. The in situ HT-XRD and TG/DTA-MS studies further declare that there is some residual carbonate on the surface of composite metal oxide in fact. After the maximal value, the loss in conversion for the calcined catalysts can be primarily

Table 3 Total pore volume and surface area of N_2 adsorption and phenol conversion for calcined Cu/Zn/Mn/Fe/Al-LDHs at different temperature

Sample	Temperature (°C)	SSA (m^2/g)	Total pore volume (cc/g)	Phenol conversion (%)
Cu-LDH1	400	47	0.83	54
	440	51	0.59	66
	500	44	0.34	73
	600	50	0.51	71
	700	48	0.40	70
Cu-LDH2	400	78	0.69	66
	440	74	0.66	51
	500	76	0.62	100
	600	37	0.62	52
	700	23	0.34	70
Cu-LDH3	400	107	0.67	13
	440	90	0.62	21
	500	245	1.25	15
	600	57	0.52	9
	700	33	0.38	7

due to the growth of spinel-like phase coupled with the removal of residual carbonate. This suggests that the acidic surface of the solid offered by residual carbonate may be another reason for increasing the phenol conversion by obtaining intermediate compound [60]. Compared with the conversions of phenol on samples calcined at 500 °C, it can be observed that the highest conversion is 100% for Cu-LDH2, followed by 73% for Cu-LDH1 and 15% for Cu-LDH3 after reaction period of one hour. The significant difference may be related to the different synergy among transition metal ions. We should be cautious in dealing with the detrimental effect on the catalytic activity of the introduction of Mn element. This also arouses the interest of our further studies on them. At least the introduction of Mn element may improve the stability of catalyst [29, 30]. In addition, it is also quite promising to find out the basic reason for the increasing catalytic activity of Cu-LDH2 and the decreasing catalytic activity of Cu-LDH3 calcined at 500 °C by further comparison of their structure and performance.

Conclusions

Three carbonate layered double hydroxides (LDHs) with different initial Cu/Zn/Mn/Fe/Al atomic ratios of 1/1/0/0/1, 1/1/0/0.3/0.7, and 1/0.7/0.3/0.3/0.7 can be obtained by the coprecipitation method. This is the first description in the literature of thermal evolution of LDHs materials containing simultaneously Cu^{2+}, Zn^{2+}, Mn^{2+}, Fe^{3+}, and Al^{3+}. Thermal stability of the lamellar structure of Cu-based LDHs decrease with Al^{3+} and Zn^{2+} ion being partially, respectively, substituted by Fe^{3+} and Mn^{2+} ion and the thermal decomposition of precursor in air is more facile than in nitrogen. On the one hand, the high M–O bond energy of Fe–O and Mn–O and the low octahedral crystal field stabilization energy (CFSE) of Fe^{3+} and Mn^{2+} ion can lead to the facile thermal decomposition of precursor. On the other hand, the high formation heat of Fe- and Mn-containing metal oxide impels the formation of thermodynamically stable composite metal oxide phases even at low temperatures. Thermal analysis of these samples also showed a significant thermal effect variation depending on the nature of the atmosphere, especially at higher temperatures, owing to the exothermic effect during the formation of composite metal oxides with various oxidation states and composite forms of transition metal ions and the structural rearrangement. Both the phase structures and composition of calcined LDHs influence textural properties and the catalytic liquid-phase oxidation of aqueous phenol solutions. The highest activity is 100% for LDH calcined at 500 °C with Cu/Zn/Mn/Fe/Al atomic ratios of 1/1/0/0.3/0.7, which is mainly related to the formation of a larger amount of composite metal oxide with some residual carbonate in the solid. It is necessary to further study the three catalysts in the phenol oxidation with hydrogen peroxide.

Acknowledgements We gratefully thank the financial support from the National Natural Science Foundation of China (Grant No. 20901056) and 973 Program (2009CB939802).

References

1. De Roy A, Fornao C, Besse JP (2001) In: Rives V (ed) Layered double hydroxides: present and future. Nova Science, New York, p 1
2. Evans DG, Slade RCT (2006) In: Duan X, Evans DG (eds) Structure and bonding, vol 119. Springer Verlag, Berlin, p 1
3. Cavani F, Trifiro F, Vaccari A (1991) Catal Today 11:173
4. Basile F, Vaccari A (2001) In: Rives V (ed) Layered double hydroxides: present and future. Nova Science, New York, p 285
5. Feng L, Duan X (2006) In: Duan X, Evans DG (eds) Structure and bonding, vol 119. Springer Verlag, Berlin, p 193
6. Kannan S (2006) Catal Surv Asia 10:117
7. Serwicka EM, Bahranowski K (2004) Catal Today 90:85
8. Tichit D, Coq B (2003) CATTECH 7:206
9. Sels BF, De Vos DE, Jacobs PA (2001) Catal Rev Sci Eng 43:443
10. Bellotto M, Rebours B, Clause O, Lynch J, Bazin D, Elkaïm E (1996) J Phys Chem 100:8535
11. Hibino T, Yamashita Y, Kosuge K, Tsunashima A (1995) Clays Clay Miner 43:427
12. Hudson MJ, Carlino S, Apperley DC (1995) J Mater Chem 5:323
13. Belloto M, Rebours B, Clause O, Lynch J, Bazin D, Elkaïm E (1996) J Phys Chem 100:8527
14. Kooli F, Crespo I, Barriga C, Ulibarri MA, Rives V (1996) J Mater Chem 6:1199
15. Kovanda F, Jirátová K, Rymeš J, Koloušek D (2001) Appl Clay Sci 18:71
16. Reichle WT, kang SY, Everhardt DS (1986) J Catal 101:352
17. Ulibarri MA, Fernández JM, Labajos FM, Rives V (1991) Chem Mater 3:626
18. Pesic L, Salipurovic S, Markovic V, Vucelic D, Kagunya W, Jones W (1992) J Mater Chem 2:1069
19. Zhang LH, Li F, Evans DG, Duan X (2004) Mater Chem Phys 87:402
20. StG Christoskova, Stoyanova M, Georgieva M (2001) Appl Catal A 208:243
21. Pintar A, Levec J (1992) Chem Eng Sci 47:2395
22. Luck F (1996) Catal Today 27:195
23. Levec J, Pintar A (1995) Catal Today 24:51
24. Dubey A, Kannan S, Velu S, Suzuki K (2003) Appl Catal A 238:319
25. Dubey A, Rivesb V, Kannan S (2002) J Mol Catal A 181:151
26. Resini C, Catania F, Berardinelli S, Paladino O, Busca G (2008) Appl Catal B 84:678
27. Yoon CH, Cho SH, Kim SH, Ha SR (2001) Water Sci Technol 43:229
28. Belkacemi K, Larachi F, Hamoudi S, Sayari A (2000) Appl Catal A 199:199
29. Kim KH, Kim JR, Ihm SK (2009) J Hazard Mater 167:1158
30. Bhargava S, Jani H, Tardio J, Akolekar D, Hoang M (2007) Ind Eng Chem Res 46:8652
31. Tichit D, Lhouty MH, Guida A, Chiche BH, Figueras F, Auroux A, Bartalini D, Garrone E (1995) J Catal 151:50
32. Corma A, Fornés V, Rey F (1994) J Catal 148:205
33. Li F, Zhang LH, Evans DG, Duan X (2004) Colloids Surf A 244:169

34. Zhang LH, Zheng C, Li F, Evans DG, Duan X (2008) J Mater Sci 43:237. doi:10.1007/s10853-007-2167-8
35. Zhang LH, Xiang X, Zhang L, Li F, Zhu J, Evans DG, Duan X (2008) J Phys Chem Solids 69:1098
36. Vaccari A (1998) Catal Today 41:53
37. Kanezaki E (1998) Inorg Chem 37:2588
38. Del Arco M, Malet P, Trujillano R, Rives V (1999) Chem Mater 11:624
39. Rocha J, Del Arco M, Rives V, Ulibarri MA (1999) J Mater Chem 9:2499
40. Tichit D, Bennani MN, Figueras F, Ruiz JR (1998) Langmuir 14:2086
41. Dean JA (1991) Lange's handbook of chemistry, 13th edn. Science, Beijing
42. Barin I, Knacke O (1973) Thermochemical properties of inorganic substances. Springer Verlag, Berlin
43. Barin I, Knacke O, Kubashewski O (1977) Thermochemical properties of inorganic substances, supplement. Springer Verlag, Berlin
44. Kannan S, Rives V, Knözinger H (2004) J Solid State Chem 177:319
45. Kannan S, Dubey A, Knözinger H (2005) J Catal 231:381
46. Barriga C, Jones W, Malet P, Rives V, Ulibarri MA (1998) Inorg Chem 37:1812
47. Li F, Liu JJ, Evans DG, Duan X (2004) Chem Mater 16:1597
48. Radha AV, Thomas GS, Kamath PV, Shivakumara C (2007) J Phys Chem B 111:3384
49. Britto S, Radha AV, Ravishankar N, Kamath PV (2007) Solid State Sci 9:279
50. Barriga C, Fernández JM, Ulibarri MA, Labajos FM, Rives V (1996) J Solid State Chem 124:205
51. Rojas R, Ulibarri MA, Barriga C, Rives V (2008) Microporous Mesoporous Mater 112(1–3):262
52. Holgado MJ, San Román S, Malet P, Rives V (2005) Mater Chem Phys 89:49
53. Rives V (2001) In: Rives V (ed) Layered double hydroxides: present and future. Nova Science, New York, p 115
54. Labajos FM, Sastre MD, Trujillano R, Rives V (1999) J Mater Chem 9:1033
55. Béres A, Pálinkó I, Fudala Á, Kiricsi I, Kiyozumi Y, Mizukami F, Nagy JB (1999) J Therm Anal Calorim 56:311
56. Kagunya W, Dutta PK, Lei Z (1997) Physica B 234:910
57. Yan H, Lu J, Wei M, Ma J, Li H, He J, Evans DG, Duan X (2008) J Mol Struct THEOCHEM 866:34
58. Labajos FM, Rives V, Ulibarri MA (1992) J Mater Sci 27:1546. doi:10.1007/BF00542916
59. Kannan S, Narayanan A, Swamy CS (1996) J Mater Sci 31:2353. doi:10.1007/BF01152946
60. Hočevar S, Batista J, Levec J (1999) J Catal 184:39